Modelling and Operation of 6-Pulse Thyristor Rectifiers for supplying High Power Electrolyzers

Alvaro Iribarren
Institute of Smart Cities (ISC)
Dept. of Electrical, Electronic and Communications Engineering
Public University of Navarre
Campus de Arrosadía
31006 Pamplona, Spain
alvaro.iribarren@unavarra.es

Ernesto L. Barrios
Institute of Smart Cities (ISC)
Dept. of Electrical, Electronic and Communications Engineering
Public University of Navarre
Campus de Arrosadía
31006 Pamplona, Spain
ernesto.barrios@unavarra.es

Harkaitz Ibaiondo
Ingeteam Power Technology
Zamudio, Spain
Harkaitz.Ibaiondo@ingeteam.com

Alain Sanchez-Ruiz
Ingeteam R&D Europe
Zamudio, Spain
Alain.Sanchez@ingeteam.com

Joseba Arza
Ingeteam R&D Europe
Zamudio, Spain
joseba.arza@ingeteam.com

Pablo Sanchis
Institute of Smart Cities (ISC)
Detp. of Electrical, Electronic and Communications Engineering
Public University of Navarre
Campus de Arrosadia
31006 Pamplona, Spain
pablo.sanchis@unavarra.es

Alfredo Ursúa
Institute of Smart Cities (ISC)
Dept. of Electrical, Electronic and Communications Engineering
Public University of Navarre
Campus de Arrosadia
31006 Pamplona, Spain
alfredo.ursua@unavarra.es

***Abstract*—This paper presents a detailed analysis of a 6-pulse thyristor rectifier aimed at supplying high power electrolyzers. For this purpose, an analytical model of the three-phase controlled rectifier with AC-side inductance and constant-voltage load has been developed. The different operating modes are identified and characterized. The derived equations are then combined with the electrical model of the electrolyzer, which allows to predict the operating point of the system. This model may serve as a useful tool for dimensioning thyristor rectifiers when operating with high power electrolyzers.**

Keywords—Thyristor rectifiers, Three-phase controlled rectifier, High power electrolyzer, Water electrolysis, Analytical Model

I. INTRODUCTION

Green hydrogen arises as one of the main possible energy vectors of the twenty-first century and is expected to play a pivotal role in this transition towards a carbon-free energy system [1]. Water electrolysis supplied by renewable electricity stands as the main solution for the production of green hydrogen. In particular, alkaline electrolysis (AEL) and proton exchange membrane electrolysis (PEMEL) are nowadays the most mature and developed technologies for high-power applications [2]. These electrolyzers need to be supplied with DC voltages and currents, as hydrogen production from water electrolysis is directly related to the DC component of the current that flows through the electrolyzer according to Faraday's law of electrolysis [3].

AC-DC converters are currently used for feeding electrolyzers directly from the power grid. Large current rectifiers are required for these applications, as industrial scale electrolyzers present very high DC current demands (up to thousands of Amperes) with relatively low DC voltages (hundreds of Volts) [4]. Regarding the electrolyzer electrical behavior, it operates as a constant-voltage load in series with an impedance with ohmic and capacitive dynamics [5].

Commonly these rectifiers include a DC inductance in order to filter the output current [4,6,7], but this significantly increases the overall cost of the system due to the large DC currents that these inductances need to handle. In contrast to this, the present study demonstrates that the thyristor rectifier can indeed be directly connected to a constant-voltage load with no major operation concerns, thus avoiding the use of a DC side inductance and reducing the overall cost of the system.

In this case of a constant-voltage load, the well-known expression for the rectified voltage V_{DC} as a function of the cosine of the thyristors' firing angle α [8] is no longer valid, therefore a new analytical model for this kind of operation should be developed. Furthermore, AC-side inductances L_{AC} are normally used in order to filter the harmonic content of the grid currents and comply with the limits established by international regulations such as IEEE 519-2014. When operating the system under load, these inductances modify the voltage range obtained at the DC output of the rectifier. In [9], a modified equation that takes into account the effect of L_{AC} on the rectified voltage V_{DC} is proposed, but in this analysis a constant-current load is considered. Little information about the operational behavior of thyristor rectifiers supplied from an inductive AC source and driving a constant-voltage load can be found in literature, as most treatments of three-phase rectifiers only consider operation with inductive (or constant-current) loading [10]. An analysis of three phase diode bridge rectifiers operating with constant-voltage load can be found in [10], but only focusing on the continuous AC-side conduction mode. This analysis is expanded in [11], where the discontinuous conduction modes are studied. This same approach is followed in [12]. Still, to the best of the authors' knowledge, few detailed analysis of thyristors-based rectifiers with constant-voltage load can be found in literature, and none regarding the operation together with an electrolyzer.

The aim of this work is to study the operation of three-phase thyristor rectifiers used for feeding high power electrolyzers. For this purpose, an analytical model of a six-pulse thyristor rectifier with AC-side inductance and constant-voltage load is first presented in Section II, in which the different conduction modes are identified and characterized. Then, in Section III a methodology is proposed to extend this analysis in order to study the interaction between the thyristor

rectifier and the electrolyzer. This model is validated by simulation using real data from a 5.5 MW electrolyzer. This validation, as well as an explanation of some key dimensioning considerations to take into account for the design of the rectifier connected to the electrolyzer, are presented in Section IV. It is demonstrated that the grid voltage required to feed the electrolyzer is higher than the values predicted by the thyristor models available in literature. Finally, in Section V the main conclusions are summed up.

II. 6-Pulse Thyristor Bridge Rectifier with Constant-Voltage Load

A. System Description

The equivalent circuit of a 6-pulse thyristor rectifier with an AC-side inductance L_{AC} and a constant-voltage load V_{DC} is shown is Fig. 1. A three-phase balanced system is considered, where the open-circuit voltage of phase A presents the following expression:

$$e_a = \sqrt{2}E\ sin(\omega t + \varphi) \tag{1}$$

being E the RMS value of the grid phase voltage and φ the lag angle of the grid current i_a with respect to e_a. Finally, α represents the firing angle of the thyristors. Since the system is balanced, only phase A is henceforth studied.

B. Identification of Conduction Modes

Depending on the values of E, L_{AC}, V_{DC} and α, the grid current i_a and the rectified current I_{DC} will either be continuous or discontinuous, resulting in different conduction modes and different possible thyristor states combinations. These conduction modes are identified as follows:

- Continuous conduction mode (CCM): The source current i_a is continuous, thus at every moment there are three thyristors conducting (one for each phase), and each thyristor conducts for π radians. The rectified current I_{DC} is also continuous.
- Discontinuous conduction mode (DCM): The source current i_a is discontinuous. This mode can itself be divided into two: DCM-1, where the rectified current I_{DC} is continuous and where within a cycle of the fundamental frequency there are intervals where either 2 or 3 thyristors are conducting; and DCM-2, where the rectified current I_{DC} is discontinuous and where within a cycle there are intervals where either none or 2 thyristors are conducting.
- Non-conduction mode (NCM): Both source and rectified currents are zero, no thyristor is conducting at any moment.

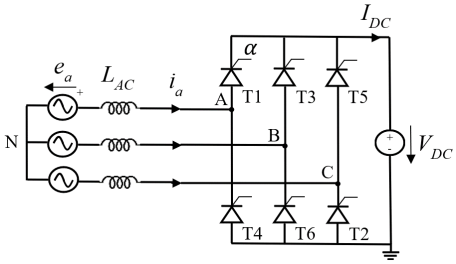

Fig. 1. 6-pulse thyristor rectifier with AC-side reactance and constant voltage load.

Examples of current waveforms in these conduction modes are shown in Fig. 2, which are obtained for E = 370 V, V_{DC} = 500 V, and L_{AC} = 30 µH, with different firing angles.

C. Grid Current Equations

The expressions for the AC-side source current i_a can be deduced from a simple circuit with two voltage sources, namely voltages e_a and v_{AN}, and the AC-side inductance L_{AC}, as shown in Fig. 3. The voltage v_{AN} is defined by the conducting thyristors, which depend on the conduction mode,

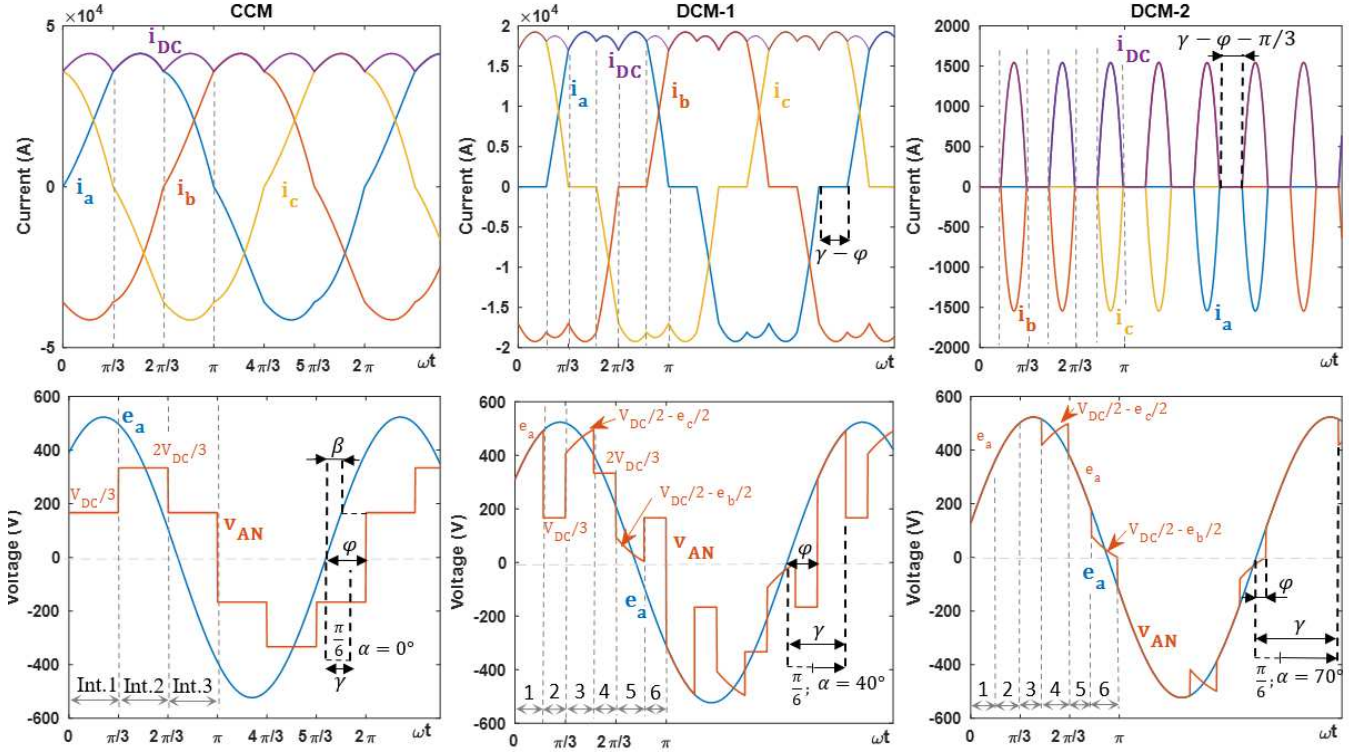

Fig. 2. Voltage and current waveforms in CCM, DCM-1 and DCM-2, corresponding to firing angles of 0, 40 and 70 degrees, respectively.

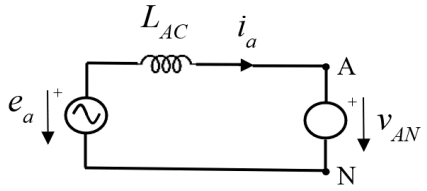

Fig. 3. Equivalent circuit for current calculation.

resulting in different equations for i_a for every conduction mode.

When there are 3 thyristors conducting (one for each phase), which happens always in CCM and during certain intervals in DCM-1, the voltage v_{AN} can be computed as:

$$if\ i_a, i_b, i_c \neq 0, \rightarrow v_{AN} = (2u_1 - u_3 - u_5)\, V_{DC}/3 \quad (2)$$

where u_1, u_3 and u_5 are the connection functions of T1, T3 and T5, respectively (1 while conducting and 0 while switched off).

If instead of this, the current is zero in one of the phases, that is when only two thyristors are conducting, expression (2) is no longer valid. This happens during certain intervals of DCM-1 and in DCM-2. In this case, the fact that the current is zero in one of the phases can be taken into account to calculate the voltage v_{AN}. If phase A is the one that is not conducting, with thyristors T1 and T4 switched off, then v_{AN} is equal to the open circuit voltage e_a, as no current is flowing through this phase's inductance.

$$if\ i_a = 0\ \rightarrow v_{AN} = e_a \quad (3)$$

If instead, one of the other two remaining phases is the one that is not conducting, then v_{AN} is computed as:

$$if\ i_a \neq 0, i_b | i_c = 0\ \rightarrow v_{AN} = \left(u_1 - \frac{1}{2}\right) V_{DC} - \frac{e_k}{2} \quad (4)$$

being e_k the open circuit voltage of the phase that is not conducting, i.e., either phase B or phase C.

The procedure to determine the expressions for i_a is as follows: first, the intervals within a cycle of the fundamental frequency when the conducting thyristors change due to the commutations need to be identified; then, the voltage v_{AN} during each interval can be computed as a function of the conducting thyristors; finally, the expressions for i_a can be derived by solving the following differential equation:

$$L_{AC} \frac{di_a}{dt} = e_a - v_{AN} \quad (5)$$

Because of symmetry, the current is determined for $0 < \omega t < \pi$, that is, the positive half-cycle of i_a (flowing through thyristor T1). The current initial value is set to 0, and the lag angle φ can be calculated thanks to the following condition:

$$i_a(\omega t = \pi) = 0 \quad (6)$$

For thyristor T1 to start conducting, two conditions must be met: e_a must be greater than $V_{DC}/3$, and the thyristor firing pulse must be triggered. As the firing angle α for T1 is defined from the moment that the line voltage e_{ac} is greater than 0 (following the natural order of commutation), and this line voltage lags the phase voltage e_a by $\pi/6$ radians, it is convenient to define the following angles which can help to identify the different intervals during the positive semi-period and solve the differential equation (5):

$$\beta = sin^{-1}\left(\frac{V_{DC}}{3\sqrt{2}E}\right) \quad (7)$$

$$\gamma = max\left(\alpha + \frac{\pi}{6}, \beta\right) \quad (8)$$

where β is the angle for which $e_a = V_{DC}/3$, and γ is the angle of e_a at which T1 can start to conduct. The relationship between angles γ and φ determines the conduction mode.

1) Continuous Conduction Mode (CCM)

If angle γ is lower than the lag angle φ, T1 starts conducting just at the moment when the negative current i_a vanishes through T4, therefore i_a is continuous and the thyristor rectifier is operating in CCM. For solving the differential equation (5) in this mode, three different intervals are identified in the semi-period, with different thyristors conducting and therefore different v_{AN} values. The duration of these intervals, the conducting thyristors, the v_{AN} values and the equations for i_a corresponding to each of them are summarized in table I.

2) Discontinuous Conduction Mode 1 (DCM-1)

If γ is greater than φ, the current through thyristor T4 vanishes before T1 can start conducting, therefore i_a is discontinuous. The angle during which the grid current is zero is equal to $\gamma - \varphi$. In discontinuous conduction mode two cases can occur: if γ is lower than $\varphi + \pi/3$, then T1 can start conducting before the current flowing through the other two phases (B and C) fades, therefore the output current is continuous. This is the case of DCM-1. In this mode, six intervals are identified in a semi-period. The duration of these intervals, the conducting thyristors, the v_{AN} values and the equations for i_a corresponding to each of them are summarized in table II.

TABLE I. CCM INTERVALS DURING THE POSITIVE SEMI-PERIOD

CONTINUOUS CONDUCTION MODE				
Interval	**Duration**	**Conducting thyristors**	v_{AN}	$i_a(\omega t)$
1	$0 < \omega t < \frac{\pi}{3}$	T1, T5, T6	$\frac{V_{DC}}{3}$	$\frac{\sqrt{2}E}{\omega L}[cos(\varphi) - cos(\omega t + \varphi)] - \frac{V_{DC}\omega t}{3\omega L}$ (9)
2	$\frac{\pi}{3} < \omega t < \frac{2\pi}{3}$	T1, T2, T6	$\frac{2V_{DC}}{3}$	$\frac{\sqrt{2}E}{\omega L}[cos(\varphi) - cos(\omega t + \varphi)] + \frac{V_{DC}}{3\omega L}\left(\frac{\pi}{3} - 2\omega t\right)$ (10)
3	$\frac{2\pi}{3} < \omega t < \pi$	T1, T2, T3	$\frac{V_{DC}}{3}$	$\frac{\sqrt{2}E}{\omega L}[cos(\varphi) - cos(\omega t + \varphi)] - \frac{V_{DC}}{3\omega L}\left(\omega t + \frac{\pi}{3}\right)$ (11)

TABLE II. DCM-1 INTERVALS DURING THE POSITIVE SEMI-PERIOD

DISCONTINUOUS CONDUCTION MODE 1					
Interval	**Duration**	**Conducting thyristors**	v_{AN}	$i_a(\omega t)$	
1	$0 < \omega t < \gamma - \varphi$	T5, T6	e_a	0	(12)
2	$\gamma - \varphi < \omega t < \frac{\pi}{3}$	T1, T5, T6	$\frac{V_{DC}}{3}$	$\frac{\sqrt{2}E}{\omega L}[cos(\gamma) - cos(\omega t + \varphi)] + \frac{V_{DC}}{3\omega L}(\gamma - \varphi - \omega t)$	(13)
3	$\frac{\pi}{3} < \omega t < \frac{\pi}{3} + \gamma - \varphi$	T1, T6	$\frac{V_{DC}}{2} - \frac{e_c}{2}$	$\frac{\sqrt{2}E}{\omega L}\left[cos(\gamma) - \frac{1}{2}cos(\varphi) - cos(\omega t + \varphi) - \frac{1}{2}cos\left(\omega t + \varphi + \frac{2\pi}{3}\right)\right] + \frac{V_{DC}}{6\omega L}\left(2\gamma - 2\varphi - 3\omega t + \frac{\pi}{3}\right)$	(14)
4	$\frac{\pi}{3} + \gamma - \varphi < \omega t < \frac{2\pi}{3}$	T1, T2, T6	$\frac{2V_{DC}}{3}$	$\frac{\sqrt{2}E}{\omega L}\left[\frac{3}{2}cos(\gamma) - \frac{1}{2}cos(\varphi) - cos(\omega t + \varphi)\right] + \frac{V_{DC}}{6\omega L}\left(3\gamma - 3\varphi - 4\omega t + \frac{2\pi}{3}\right)$	(15)
5	$\frac{2\pi}{3} < \omega t < \frac{2\pi}{3} + \gamma - \varphi$	T1, T2	$\frac{V_{DC}}{2} - \frac{e_b}{2}$	$\frac{\sqrt{2}E}{\omega L}\left[\frac{3}{2}cos(\gamma) - cos(\omega t + \varphi) - \frac{1}{2}cos\left(\omega t + \varphi - \frac{2\pi}{3}\right)\right] + \frac{V_{DC}}{2\omega L}(\gamma - \varphi - \omega t)$	(16)
6	$\frac{2\pi}{3} + \gamma - \varphi < \omega t < \pi$	T1, T2, T3	$\frac{V_{DC}}{3}$	$\frac{\sqrt{2}E}{\omega L}[cos(\gamma) - cos(\omega t + \varphi)] + \frac{V_{DC}}{3\omega L}\left(\gamma - \varphi - \omega t - \frac{\pi}{3}\right)$	(17)

TABLE III. DCM-2 INTERVALS DURING THE POSITIVE SEMI-PERIOD

DISCONTINUOUS CONDUCTION MODE 2					
Interval	**Duration**	**Conducting thyristors**	v_{AN}	$i_a(\omega t)$	
1	$0 < \omega t < \gamma - \varphi - \frac{\pi}{3}$	None	e_a	0	(18)
2	$\gamma - \varphi - \frac{\pi}{3} < \omega t < \frac{\pi}{3}$	T5, T6	e_a	0	(19)
3	$\frac{\pi}{3} < \omega t < \gamma - \varphi$	None	e_a	0	(20)
4	$\gamma - \varphi < \omega t < \frac{2\pi}{3}$	T1, T6	$\frac{V_{DC}}{2} - \frac{e_c}{2}$	$\frac{\sqrt{2}E}{\omega L}\left[cos(\gamma) + \frac{1}{2}cos\left(\gamma + \frac{2\pi}{3}\right) - cos(\omega t + \varphi) - \frac{1}{2}cos\left(\omega t + \varphi + \frac{2\pi}{3}\right)\right] + \frac{V_{DC}}{2\omega L}(\gamma - \varphi - \omega t)$	(21)
5	$\frac{2\pi}{3} < \omega t < \frac{\pi}{3} + \gamma - \varphi$	None	e_a	0	(22)
6	$\frac{\pi}{3} + \gamma - \varphi < \omega t < \pi$	T1, T2	$\frac{V_{DC}}{2} - \frac{e_b}{2}$	$\frac{\sqrt{2}E}{\omega L}\left[cos\left(\gamma + \frac{\pi}{3}\right) + \frac{1}{2}cos\left(\gamma - \frac{\pi}{3}\right) - cos(\omega t + \varphi) - \frac{1}{2}cos\left(\omega t + \varphi - \frac{2\pi}{3}\right)\right] + \frac{V_{DC}}{2\omega L}\left(\gamma - \varphi - \omega t + \frac{\pi}{3}\right)$	(23)

3) Discontinuous Conduction Mode 2 (DCM-2)

In the other case, if γ is greater than $\varphi + \pi/3$, then the current flowing through phases B and C reaches zero before T1 is activated, and thus the output rectified current is discontinuous as well. This is the case of DCM-2. The angle during which all the thyristors are switched off and the output current is zero is equal to γ - φ - $\pi/3$. Again, six intervals are identified in a semi-period. The duration of these intervals, the conducting thyristors, the v_{AN} values and the equations for i_a corresponding to each of them are summarized in table III.

Fig. 2 shows voltages e_a and v_{AN}, and currents i_a, i_b, i_c and i_{DC}, in the different conduction modes. These are obtained for E = 370 V, V_{DC} = 500 V, and L_{AC} = 30 µH, with three different firing angles: 0º, 40º and 70º. Angles β, γ and φ are also identified. It can be observed how these angles fulfill the conditions explained above for every conduction mode.

D. Boundaries between Conduction Modes

- Boundary between CCM and DCM-1, defined by the following condition:

$$\gamma_{crit,1} = \varphi \tag{24}$$

By applying the boundary condition (6) to equation (11) the lag angle φ in CCM can be calculated. Then using (24) and transforming γ back to the firing angle α using (8), it yields:

$$\alpha_{crit,1} = cos^{-1}\left(\frac{\sqrt{2}\pi V_{DC}}{9E}\right) - \frac{\pi}{6} \quad (25)$$

- Boundary between DCM-1 and DCM-2, defined by the following condition:

$$\gamma_{crit,2} = \varphi + \frac{\pi}{3} \quad (26)$$

By applying the boundary condition (6) to equation (17) the lag angle φ in DCM-1 can be calculated. Then using (26) and transforming γ back to the firing angle α using (8), it yields:

$$\alpha_{crit,2} = cos^{-1}\left(\frac{\pi V_{DC}}{3\sqrt{6}E}\right) \quad (27)$$

- Boundary between DCM-2 and NCM: if the firing angle, and consequently angle γ, is increased to a value where the difference between the open circuit voltages of the two phases to which it corresponds to conduct in the moment of the firing pulse is below V_{DC}, the rectifier is not able to conduct at any time. This is defined by the following conditions, which are in fact equivalent:

$$e_a(\gamma) = e_b(\gamma) + V_{DC} \quad (28)$$

$$e_a\left(\gamma + \frac{\pi}{3}\right) = e_c\left(\gamma + \frac{\pi}{3}\right) + V_{DC} \quad (29)$$

By applying the boundary condition (6) to either (21) or (23), as they yield the same result, the lag angle φ in DCM-2 can be calculated. Then using (28) or (29) and transforming γ back to the firing angle α using (8), it yields:

$$\alpha_{MNC} = \frac{2\pi}{3} - sin^{-1}\left(\frac{V_{DC}}{\sqrt{6}E}\right) \quad (30)$$

Another boundary between DCM-2 and NCM exist at $V_{DC} = \sqrt{6}E$, as this is the peak line-to-tine voltage. For greater V_{DC} values the rectifier cannot conduct either.

As it can be seen, these boundaries depend exclusively on the values of E and V_{DC}, and are independent of the line inductance L_{AC}. Fig. 4 shows the different conduction regions of the 6-pulse thyristor rectifier as a function of α and V_{DC}, for the case of E = 370 V.

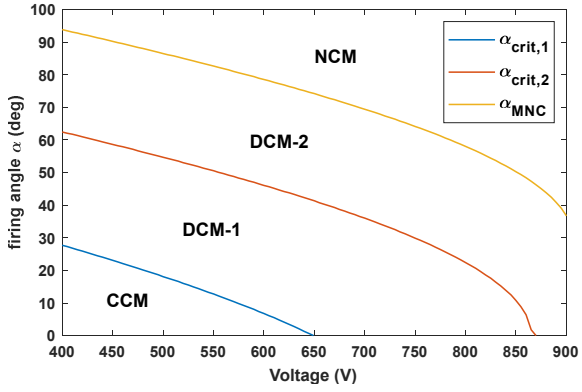

Fig. 4. Conduction regions of the 6-pulse thyristor rectifier as a function of the load DC voltage and the thyristor firing angle, for $E = 370\ V$.

E. Rectified Current I_{DC} Calculation

It can be observed that during interval $\omega t \in \{\pi/3\,, 2\pi/3\}$ the grid current i_a equals the rectified current I_{DC}. Therefore, I_{DC} can be calculated as follows:

$$I_{DC} = \frac{3}{\pi}\int_{\pi/3}^{2\pi/3} i_a(\omega t)\, d(\omega t) \quad (31)$$

The calculation of this I_{DC} value is of special importance in electrolysis applications, as the produced hydrogen is directly proportional to the DC component of the current that flows through the electrolyzer.

III. 6-Pulse Thyristor Bridge Rectifier with Electrolyzer

In order to analyze the interaction between the thyristor rectifier and the electrolyzer, an electrical model of the electrolyzer is required. Most models in literature describe the electric behavior of electrolyzers by a constant-voltage load (namely the reversible voltage) in series with an ohmic resistance and a couple of RC branches that model the activation phenomena at the electrodes. For this study, the model described in [5] has been employed due to its accuracy to reproduce both the static and the dynamic behavior of the electrolyzer. Following this model, the equivalent circuit of the complete system (thyristor rectifier and electrolyzer) is shown in Fig. 5.

The steady-state operating point of the electrolyzer is defined by its polarization curve, which defines the relationship between the electrolyzer's DC current and voltage. This equation presents the following expression:

$$V_{DC} = N_s\left[V_{rev} + R_{Ohm}I_{DC} + s\,ln\left(\frac{I_{DC}}{t}+1\right) + v\,ln\left(\frac{I_{DC}}{w}+1\right)\right] \quad (32)$$

where the different parameters $(N_s, V_{rev}, R_{Ohm}, s, t, v, w)$ can be calculated following the methodology presented in [5]. By combining the expressions of the thyristor bridge rectified current (31) and the static polarization equation of the electrolyzer (32) it is possible to determine the steady-state operating point of the electrolyzer when feeded by the 6-pulse thyristor rectifier, as a function of the thyristors' firing angle.

IV. Model Validation by Simulation and Sizing Example

The electrolyzer model employed for the validation is based on real data from a 5.5 MW electrolyzer. The polarization $I-V$ curves for this electrolyzer at ambient temperature (20 ºC) and at the nominal operating temperature (70 ºC) are shown in Fig. 6. The nominal current and voltage values of this stack are 7000 A and 790 V, respectively, at 70ºC. It also presents a minimum operating current of 700 A, below which the electrolyzer is not allowed to operate due to safety reasons concerning the formation of explosive gas mixtures.

Temperature is a key variable in the operation of electrolyzers, as it present a significant influence on the electrical consumption of the stack: as temperature increases the stack voltage for the same current values decreases, as shown in Fig. 6. Therefore, the electrical efficiency for the same hydrogen generation rate is improved. Temperature effects have to be considered as well on the sizing of the electrical power supply, as the power converter will need to deliver greater power during cold operation than during

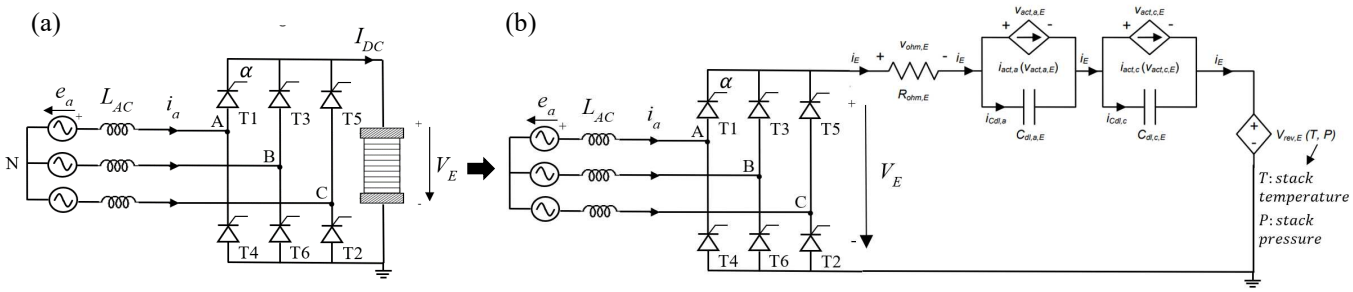

Fig. 5. (a) 6-pulse thyristor rectifier connected to the electrolyzer. (b) Equivalent circuit of the whole system (model from [5]).

operation at nominal temperature. Furthermore, this power converter has to ensure that the stack is always working within its operation limits, defined by the electrolyzer manufacturer.

In industrial applications, high power electrolyzers are usually connected to a medium voltage AC-grid. Then, a line-frequency three-phase isolation transformer is used to reduce the voltage down to the low voltage levels of the electrolyzer. The thyristor rectifier would then be connected to the secondary winding of this transformer, and its output is directly connected to the positive and negative terminals of the electrolyzer stack. As this study shows, there is no actual need to employ an inductance at the output of the thyristor rectifier, as this last one can work with a capacitive load.

The parameters E and L_{AC} of the model presented in this work need to be adjusted according to the grid and transformer characteristics (mainly rated voltage and impedances), and the possible use of additional AC-side inductances acting as passive filters. Regardless of the voltage level of the medium voltage AC-grid to which the transformer is connected, it is possible to refer all voltages and impedances to the secondary side of the transformer. Doing so, the parameter E of the model has to be equal to the nominal RMS phase voltage of the secondary winding of the transformer. This is a design parameter that should be adjusted in order to obtain the nominal DC voltage and current of the electrolyzer with a thyristor firing angle of 0 degrees. Doing so it is possible to minimize current harmonics and obtain the maximum power factor at the nominal operation point of the stack, which is a crucial aspect in thyristor rectifiers. This value of E can be determined thanks to the developed model, but first the value of L_{AC} needs to be specified.

For this validation, an AC-side grid inductance of 10% (in per unit basis) has been employed. This inductance represents the sum of the grid and the transformer leakage inductances, all referred to the secondary side of the transformer.

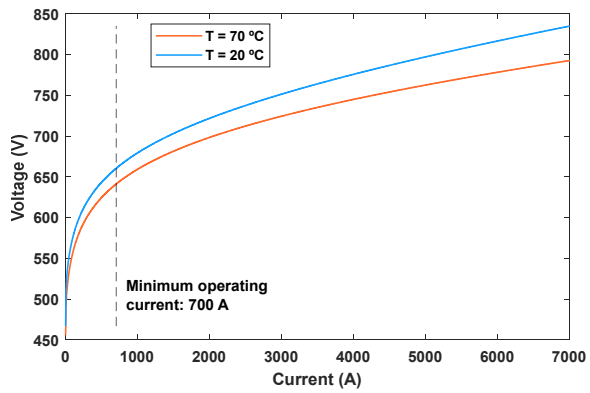

Fig. 6. Polarization $I-V$ curves of the 5.5 MW electrolyzer, at ambient temperature (20 ℃) and at the nominal operating temperature (70 ℃).

Furthermore, in order to comply with the limits established by international regulations such as IEEE 519-2014, additional AC-side inductances are usually employed for reducing grid current harmonic content. If these filtering inductances are added to the secondary windings of the transformer, the value of parameter L_{AC} of the model can be calculated as:

$$L_{AC} = L_{grid+T} + L_{filter} \tag{33}$$

where L_{grid+T} represents the sum of the grid and the transformer leakage inductances, and L_{filter} is the value of the additional filtering inductance. For the model validation, two different L_{filter} values have been analyzed: 195 µH and 65 µH. The actual values of the grid inductance L_{grid+T} in the two cases analyzed, as well as the resulting total L_{AC}, are shown in table IV.

Also, even though the model analyzed does not consider the presence of AC-side resistances, a resistance R_{AC} associated to the sum of the grid and the transformer has been included for this validation. In high power applications inductive phenomena usually dominate over resistive losses, resulting in quite high X/R ratios. For this case, an X/R ratio of 10 has been employed. The actual R_{AC} values are recorded in table IV. Again, these values are referred to the secondary side of the transformer. By adding this resistance to the validation, it is possible to check the accuracy of the model with a real AC-side impedance that includes both reactance and resistance.

Thanks to the analysis developed in section II and the methodology proposed in section III, it is possible to determine the value of E (secondary phase voltage of the transformer) required in order to obtain the nominal operation point of the electrolyzer with a thyristor firing angle of 0 degrees. To do so, the polarization curve (32) corresponding to the nominal temperature (in this case 70ºC) should be employed, as using the low-temperature curve would result in over-sizing the power converter in voltage while actually the stack will only be working at these cold temperatures for a few minutes during the start-up ramp. Following this, and using the nominal temperature polarization curve, the model predicts that a value of E = 545.0 V is required for L_{AC} = 230 µH, and E = 420.8 V for L_{AC} = 90 µH. These E values are higher than the 337.7 V that would be obtained if the classical thyristors' cosine expression [8] had been used:

$$V_{DC} = \sqrt{6}E\ cos(\alpha)\ 3/\pi \tag{34}$$

Table IV summarizes the main parameters used for the validation of the model shown in Fig. 5 for the two case studies. This model has been simulated using

MATLAB/Simulink, and firing angles sweeps from 0º down to the minimum operating current of the stack have been performed.

TABLE IV. PARAMETERS FOR THE MODEL VALIDATION

Case	L_{grid+T} (μH)	L_{filter} (μH)	L_{AC} (μH)	R_{AC} ($mOhm$)	E (V)
1	35	195	230	1.1	545.0
2	25	65	90	0.8	420.8

A. Case 1: L_{filter} = 195 μH

The electrolyzer voltage and current predicted by the model as a function of the thyristor firing angle and the simulated results are shown in Fig. 7, for both ambient and nominal temperature. Results demonstrate that the model faithfully predicts the operation point of the electrolyzer supplied by the 6-pulse thyristor rectifier. The deviations between the model and the simulated results, which are caused by the presence of R_{AC} in the simulations, are negligible. This demonstrates that neglecting the effect of the grid and transformer resistances in the model is a valid assumption for these high-power electrolysis applications.

As it can be seen in Fig. 7b, the model is able to anticipate the different conduction modes that can occur depending on α and the transition points between them. The value of L_{AC} in this case is so big that the required E voltage is very high, making the rectifier to operate in CCM between α = 0º and 13º. In this region, it is not possible to change the operating point of the electrolyzer by changing α. This is not desired as it hinders the controllability of the rectifier.

Furthermore, it can be observed in Fig. 7a that during a cold start the electrolyzer will not be able to work with the nominal current, i.e., the nominal hydrogen production. But as the stack temperature increases, the rectifier will be able to provide more and more current until the maximum 7000 A are reached with the nominal 70 ºC.

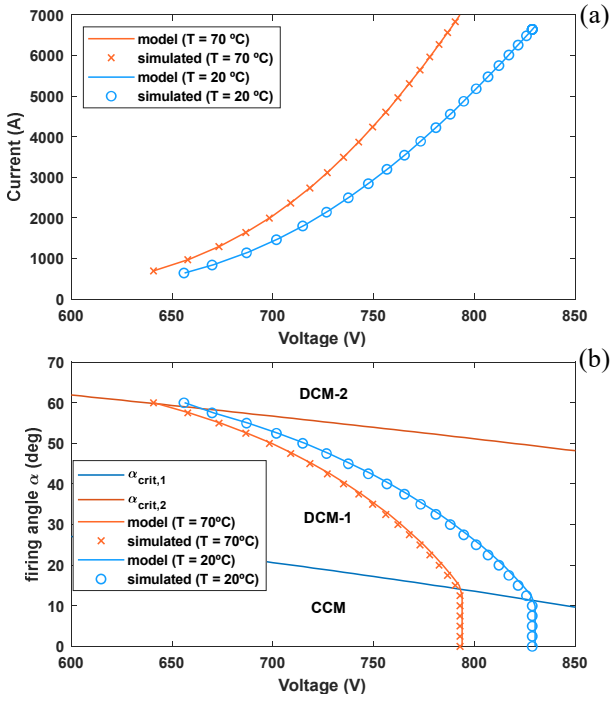

Fig. 7. Model validation with L_{filter} = 195 μH. (a) Electrolyzer $I-V$ curves. (b) Required firing angle as a function of electrolyzer voltage.

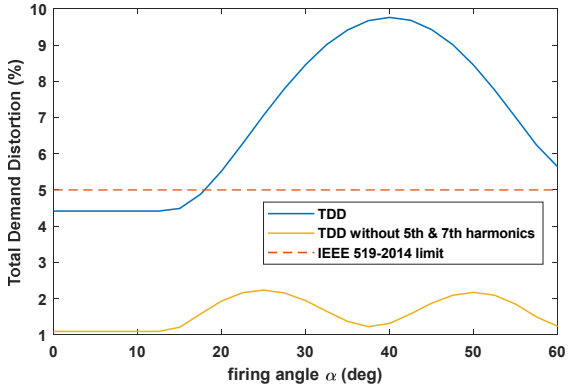

Fig. 8. Grid current total demand distortion (TDD) with L_{filter} = 195 μH and nominal operating temperature (70 ºC).

Fig. 8 shows the grid current total demand distortion (TDD) as a function of the firing angle, for this case of L_{filter}=195 µH and at the nominal operating temperature. As it can be observed, even the use of this large filtering inductance is not able to reduce the TDD below 5%, which is the limit defined in IEEE 519-2014 (the standard taken as reference for this analysis) for weak AC grids. But this harmonic distortion in mainly produced by the presence of the 5th and 7th harmonic, as this is a 6-pulse rectifier. Fig. 8 also shows the resulting TDD if these two harmonics are omitted. In this case, the TDD would fall to acceptable values below the 5% limit. Due to this, specific filters tuned for the 5th and 7th harmonics or the use of an active filter capable of canceling them seem to be very interesting solutions for these applications.

B. Case 2: L_{filter} = 65 μH

If either tuned filters or an active filter are to be used for mitigating the 5th and 7th harmonics, the passive inductance

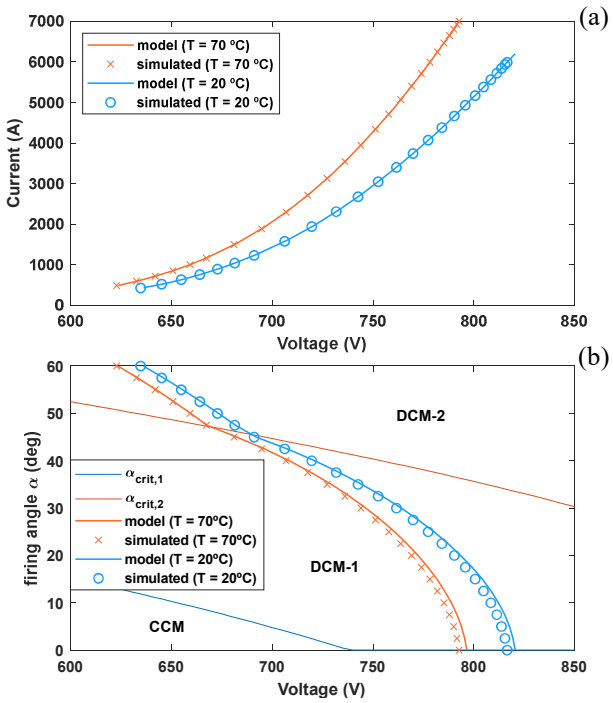

Fig. 9. Model validation with L_{filter} = 65 μH. (a) Electrolyzer $I-V$ curves. (b) Required firing angle as a function of electrolyzer voltage.

L_{filter} can be reduced down to the value with which the rest of the harmonics (11th, 13th, 17th, 19th, 23rd, 25th, etc.) generated by the 6-pulse rectifier comply with their respective limits defined in IEEE 519-2014. This inductance was found to be 65 µH, and the model has been validated again using this L_{filter} value. The electrolyzer voltage and current predicted by the model as a function of α and the simulated results are shown in Fig. 9. As in the previous case, the model is able to determine the operation point of the electrolyzer supplied by the 6-pulse thyristor rectifier with great accuracy.

With this smaller L_{filter} the required E voltage is considerably lower than in the previous case. Due to this, CCM does not appear, and the rectifier starts in DCM-1 at α=0º, therefore assuring a better controllability in the whole α range.

Fig. 10 shows the grid current total demand distortion (TDD) as a function of the firing angle, for this case of L_{filter}=65 µH. Again, if the 5th and 7th harmonics are omitted, the resulting TDD would comply with the limit defined in IEEE 519-2014 and using a much smaller inductance than in the previous case.

Finally, another obvious advantage of this solution is that due to the smaller AC-side reactance, the reactive power consumption is effectively reduced. Fig. 11 shows this reactive power consumption as a function of α, for both inductance cases, at the nominal temperature. The maximum reactive power is reduced from 6.4 MVAr to 3.6 MVAr. This can have a significant impact on the sizing of an auxiliar STATCOM, usually needed to compensate the power factor of thyristor rectifiers [4], and therefore on the cost of the whole system.

V. Conclusions

In this brief, an analysis of the operating characteristics of a 6-pulse thyristor rectifier supplying a high-power electrolyzer has been presented. For this purpose, an analytical model of the thyristor rectifier with AC-side inductances and constant-voltage load has been developed, in which the possible different conduction modes have been identified and characterized. Then, by combining the equations resulting from this analysis with the characteristic polarization curve of the electrolyzer, it has been demonstrated that it is possible to predict the steady-state operating point of the electrolyzer. This is the first time, to the best of the authors' knowledge, this interaction between a thyristor rectifier and an electrolyzer has been thoroughly studied from an analytical point of view. The applicability and usefulness of this model for the dimensioning of the complete AC-DC system integrating the rectifier and the electrolyzer has also been demonstrated.

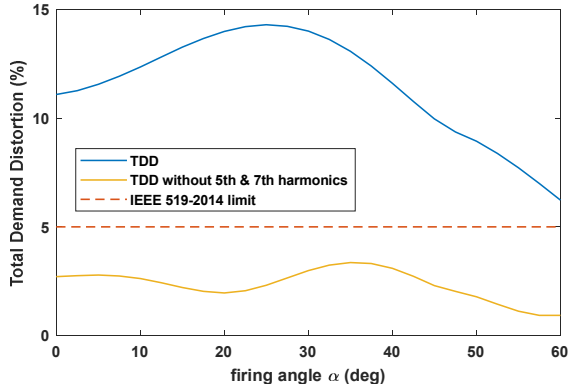

Fig. 10. Grid current total demand distortion (TDD) with L_{filter} = 65 µH and nominal operating temperature (70 ºC).

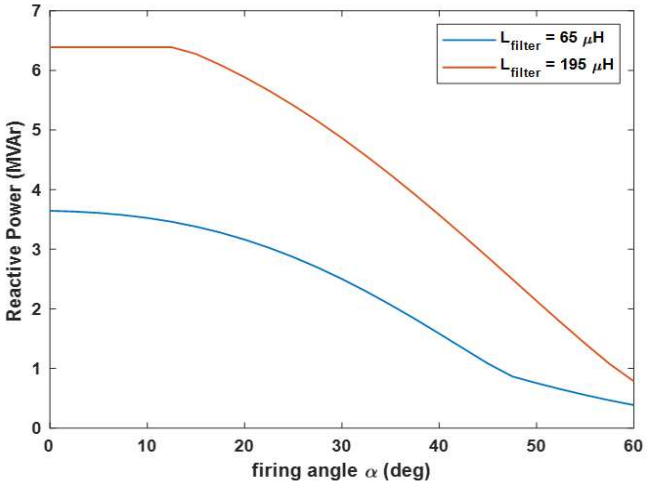

Fig. 11. Reactive power consumption at nominal operating temperature (70 ºC). Comparison between L_{filter} = 195 µH and L_{filter} = 65 µH.

References

[1] S. Shiva Kumar and V. Himabindu, "Hydrogen production by PEM water electrolysis – A review," *Mater. Sci. Energy Technol.*, vol. 2, no. 3, pp. 442–454, 2019, doi: 10.1016/j.mset.2019.03.002.

[2] O. Schmidt, A. Gambhir, I. Staffell, A. Hawkes, J. Nelson, and S. Few, "Future cost and performance of water electrolysis: An expert elicitation study," *Int. J. Hydrogen Energy*, vol. 42, no. 52, pp. 30470–30492, 2017, doi: 10.1016/j.ijhydene.2017.10.045.

[3] A. Ursúa, L. Marroyo, E. Gubía, L. M. Gandía, P. M. Diéguez, and P. Sanchis, "Influence of the power supply on the energy efficiency of an alkaline water electrolyser," *Int. J. Hydrogen Energy*, vol. 34, no. 8, pp. 3221–3233, 2009, doi: 10.1016/j.ijhydene.2009.02.017.

[4] B. Yodwong, D. Guilbert, M. Phattanasak, W. Kaewmanee, M. Hinaje, and G. Vitale, "AC-DC converters for electrolyzer applications: State of the art and future challenges," *Electron.*, vol. 9, no. 6, 2020, doi: 10.3390/electronics9060912.

[5] A. Iribarren *et al.*, "Dynamic modeling and simulation of a pressurized alkaline water electrolyzer: a multiphysics approach," pp. 1–6, 2021, doi: 10.1109/eeeic/icpseurope51590.2021.9584481.

[6] F. W. Speckmann, S. Bintz, and K. P. Birke, "Influence of rectifiers on the energy demand and gas quality of alkaline electrolysis systems in dynamic operation," *Appl. Energy*, vol. 250, no. May, pp. 855–863, 2019, doi: 10.1016/j.apenergy.2019.05.014.

[7] X. Meng, M. Chen, M. He, X. Wang, and J. Liu, "A Novel High Power Hybrid Rectifier With Low Cost and High Grid Current Quality for Improved Efficiency of Electrolytic Hydrogen Production," *IEEE Trans. Power Electron.*, vol. 37, no. 4, pp. 3763–3768, 2022, doi: 10.1109/TPEL.2021.3126725.

[8] M. Rashid, *The power electronics handbook*; Elsevier, 2011.

[9] D. J. Perrault and J. G. Kassakian, "Effects of firing angle imbalance on 12-pulse rectifiers with interphase transformers," *PESC Rec. - IEEE Annu. Power Electron. Spec. Conf.*, pp. 1075–1080, 1993, doi: 10.1109/pesc.1993.472052.

[10] V. Caliskan, D. J. Perreault, T. M. Jahns, and J. G. Kassakian, "Analysis of Three-Phase Rectifiers with Constant-Voltage Loads," *IEEE Trans. Circuits Syst. I Fundam. Theory Appl.*, vol. 50, no. 9, pp. 1220–1226, 2003, doi: 10.1109/TCSI.2003.816323.

[11] P. Pejović and J. W. Kolar, "An analysis of three-phase rectifiers with constant voltage loads," *Proc. Pap. - 5th Eur. Conf. Circuits Syst. Commun. ECCSC'10*, pp. 119–126, 2010.

[12] A. Urtasun, P. Sanchis, I. San Martín, J. López, and L. Marroyo, "Modeling of small wind turbines based on PMSG with diode bridge for sensorless maximum power tracking," *Renew. Energy*, vol. 55, pp. 138–149, 2013, doi: 10.1016/j.renene.2012.12.035.